

Communication

Modified Elliptic Integral Approach for the Forced Vibration and Sound Transmission Analysis of a Nonlinear Panel Backed by a Partitioned Cavity

Yiu-Yin Lee

Department of Architecture and Civil Engineering, City University of Hong Kong, Tat Chee Avenue, Kowloon 852, Hong Kong; bcraylee@cityu.edu.hk

Abstract: This article is the further work of previous papers and also the first study to adopt the elliptic integral approach to solve the forced nonlinear structural acoustic problem. A previous elliptic integral approach, which was only used for the free vibration analyses of various nonlinear structural acoustic problems, is modified and custom designed for conducting this forced vibration analysis. The main advantage of the proposed approach is that one elliptic cosine contains various harmonic components, while one simple cosine term only carries one particular harmonic component. That is why the proposed solution form can be more concise than those in the harmonic balance procedures. This is the first study to employ the proposed elliptic cosine solution form for the forced vibration and sound transmission of a nonlinear panel backed by a partitioned cavity. This study has two focuses: (1) the development of elliptic integral approach for solving the nonlinear structural acoustic governing equations, and (2) the effect of partitioned cavities on the forced vibration response and sound transmission loss. Moreover, a set of elliptic cosine solutions is verified by that from the modified residue harmonic balance method. A mode convergence study and a harmonic contribution analysis are also conducted.



Citation: Lee, Y.-Y. Modified Elliptic Integral Approach for the Forced Vibration and Sound Transmission Analysis of a Nonlinear Panel Backed by a Partitioned Cavity. *Mathematics* **2022**, *10*, 984. <https://doi.org/10.3390/math10060984>

Keywords: nonlinear panel vibration; structural dynamics; wave equation; elliptical integral; structural-acoustic interaction

MSC: 43-08; 35G99

Academic Editors: Ioannis Dassios and Clemente Cesarano

Received: 21 February 2022

Accepted: 17 March 2022

Published: 18 March 2022

Publisher's Note: MDPI stays neutral with regard to jurisdictional claims in published maps and institutional affiliations.



Copyright: © 2022 by the author. Licensee MDPI, Basel, Switzerland. This article is an open access article distributed under the terms and conditions of the Creative Commons Attribution (CC BY) license (<https://creativecommons.org/licenses/by/4.0/>).

1. Introduction

Over the past decades, nonlinear vibration/oscillation, and sound transmission have been hot topics for many researchers. For example, Issac et al. [1] performed a study about recent advances in sound transmission loss of sandwich and composites double panels, in which some salient explanation of the various frequency and controlled regions were given. They critically examined a number of parameter effects on the sound transmission of sandwich and composite structures. Lin et al. [2] studied the sound transmission loss across orthotropic laminates in order to understand the sound-insulating capacity at various frequencies. Experiments and numerical simulations were carried out to investigate the sound penetrating characteristics of various material and panel configurations. Thamburaj and Sun [3] presented their investigations into the optimization of sound transmission loss across anisotropic sandwich beams. The material and geometric properties of the structure were treated as the variables to maximize the sound transmission loss. Chen and Lin [4] proposed a convenient technique for evaluating angular frequency in some nonlinear oscillations. In their study, it was known that once the restoring force function was given beforehand, the period of motion was determined by an integral. The angular frequency would depend on both the period of motion and the integral. If three divisions were selected on the integration interval and the trapezoid quadrature rule was employed, a higher accurate result for the angular frequency could be achieved. Sun et al. [5] studied the

energy transfer between different modes of rectangular plate with 1:3 internal resonance. The ordinary differential equations of motion for the plate were developed using the Galerkin's method. The nonlinear frequency responses and the waveforms under specific excitation frequencies were computed. The results showed that for in-plane excitation, the internal resonance between two modes occurred when the excitation frequency was not close to any linear natural frequencies. Moreover, there are still limited studies about nonlinear panel-cavity system, which adopted the common solution methods, such as finite element method, method of multiple scales, and perturbation method (e.g., [6–10]), although a considerable amount of research work about linear panel-cavity system has been published [11–17]. Lee [18] studied the transmission loss of a nonlinearly vibrating perforated panel using the multi-level residue harmonic balance method. The effects of various parameters were investigated. However, the research problem in the study was not about panel-cavity system. Lee [19] also employed a similar harmonic balance method to study the effects of large-amplitude vibration on the pressure-dependent absorption of a structure multiple-cavity system. It was the first study to consider both the effects of large-amplitude vibration and pressure-dependent absorption. However, the work in [19] did not consider the elliptic integral approach as the solution method and not focus on the transmission loss of the panel cavity system. Recently, the elliptic integral approach was used for the free vibration analyses of various nonlinear panel-cavity systems (e.g., [20]). As aforementioned, the elliptical integral approach is modified in this paper and considers an elliptic cosine solution form for the forced vibration and sound transmission of the nonlinear panel-cavity model.

2. Theory

Figure 1 shows a nonlinear panel coupled with a partitioned cavity. The acoustic boundary conditions of the partitioned cavity are listed in the following equations [19]:

$$\frac{\partial P}{\partial x} = 0 \text{ at } x = 0 \text{ or } a/3 \text{ or } 2a/3 \text{ or } a \quad (1)$$

$$\frac{\partial P}{\partial z} = 0 \text{ at } z = c_1, x = 0 \text{ to } a/3 \quad (2)$$

$$\frac{\partial P}{\partial z} = 0 \text{ at } z = c_2, x = a/3 \text{ to } 2a/3 \quad (3)$$

$$\frac{\partial P}{\partial z} = 0 \text{ at } z = c_3, x = 2a/3 \text{ to } a \quad (4)$$

$$\frac{\partial P}{\partial y} = 0 \text{ at } y = 0 \text{ and } b \quad (5)$$

$$\frac{\partial P}{\partial z} = -\rho_a \frac{\partial^2 W(x, y, t)}{\partial t^2} \text{ at } z = 0 \quad (6)$$

where a and b are the panel width and length; c_1 , c_2 , and c_3 are the cavity depths; ρ_a is air density, 1.2 kg/m^3 ; $W(x, y, t)$ is the nonlinear transverse displacement; P is the acoustic pressure field within the cavity and the acoustic governing equation is given by [12,20]:

$$\nabla^2 P - \frac{1}{C_a^2} \frac{\partial^2 P}{\partial t^2} = 0 \quad (7)$$

where C_a is sound speed, 340 m/s .

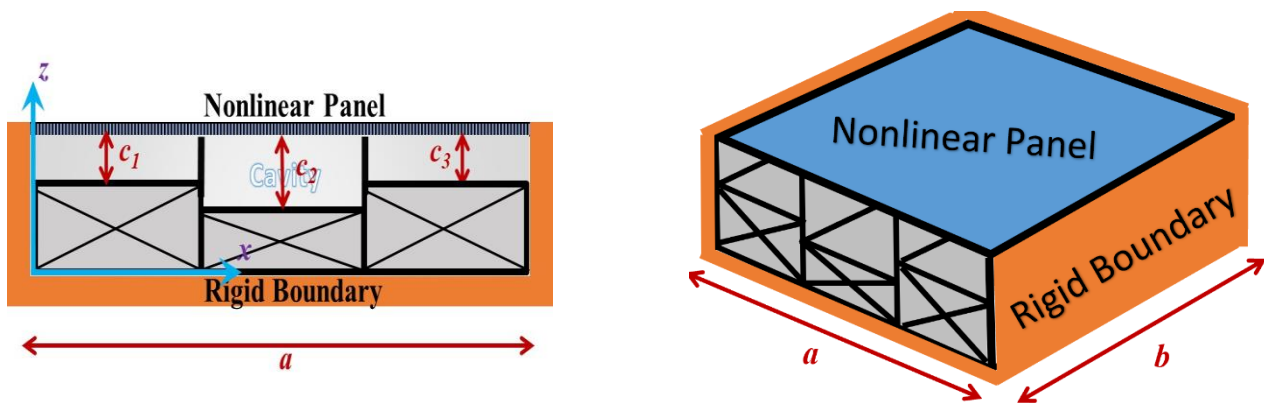


Figure 1. Nonlinear panel backed by a partitioned cavity.

By applying the boundary conditions in Equations (1)–(6) to the acoustic governing equation, the solution form of the acoustic pressure at a particular location can be obtained.

$$P(x, y, z, t) = \sum_u^U \sum_v^V (L_{uv} \sinh(\mu_{uv}z) + N_{uv} \cosh(\mu_{uv}z)) \psi_{uv}(x, y) \cos(\omega t) \quad (8)$$

where L_{uv} and N_{uv} are the coefficients depending on the boundary conditions; ψ_{uv} is the acoustic mode function, $\mu_{uv} = \frac{1}{c_a} \sqrt{\omega_{uv}^2 - \omega^2}$; u and v are acoustic mode numbers; U and V are the numbers of modes considered; ω is the driving frequency; ω_{uv} is the resonant frequency of the (u, v) mode.

Next, consider multiplying the mode shape function, and taking integration over the panel area for the pressure field in Equation (8), and obtaining the following overall acoustic pressure force:

$$P_c = \rho_a \omega^2 \sum_u^U \sum_v^V \frac{\coth(\mu_{uv}c_i)}{\mu_{uv}} \frac{(\lambda_{uv})^2 \bar{A}}{\lambda_{\psi_{uv}} \lambda_{\varphi}} \cos(\omega t) \quad (9)$$

where \bar{A} is the nonlinear panel vibration amplitude (note that $W(x, y, t) = A(t)\varphi(x, y)$); ω is the driving frequency of the external excitation; $i = 1, 2, 3$; $\lambda_{uv} = \int_0^b \int_0^a \psi_{uv} \varphi dx dy$; $\lambda_{\psi_{uv}} = \int_0^b \int_0^a \psi_{uv} \psi_{uv} dx dy$; $\lambda_{\varphi} = \int_0^b \int_0^a \varphi \varphi dx dy$. The structural and acoustic mode functions are given by [19]:

$$(x, y) = \sin\left(\frac{\pi x}{a}\right) \sin\left(\frac{\pi y}{b}\right) \quad (10)$$

$$\psi_{uv}(x, y) = \cos\left(\frac{u\pi}{a}x\right) \cos\left(\frac{v\pi}{b}y\right) \text{ at } x = 0 \text{ to } a/3 \quad (11)$$

$$\psi_{uv}(x, y) = \cos\left(\frac{u\pi}{a}\left(x - \frac{a}{3}\right)\right) \cos\left(\frac{v\pi}{b}y\right) \text{ at } x = a/3 \text{ to } 2a/3 \quad (12)$$

$$\psi_{uv}(x, y) = \cos\left(\frac{u\pi}{a}\left(x - \frac{2}{3}a\right)\right) \cos\left(\frac{v\pi}{b}y\right) \text{ at } x = 2a/3 \text{ to } a \quad (13)$$

Over the past decades, there have been many studies about Duffing equation (or Duffing oscillator) e.g., [21–25]. According to [21,22], the general Duffing equation with a harmonic forcing term is given by:

$$\frac{d^2s}{dt^2} + \alpha s + \beta s^3 + \Gamma \cos(\omega t) = 0 \quad (14)$$

where s is used as the variable in the Duffing equation; α and β are the coefficients associated with the linear and nonlinear terms, s and s^3 ; Γ = excitation magnitude.

Fundamentally, the governing equation of a nonlinear flexible panel coupled with a cavity [19,20] can be exactly the same as Equation (14) by changing the following symbols:

$$s = A \tag{15}$$

$$\alpha = \omega_0^2 \tag{16}$$

$$\beta = \frac{E\tau}{4(1-\nu^2)\rho} \left(\frac{\pi}{a}\right)^4 \left[(1+\gamma^4) \left(\frac{3}{4} - \frac{\nu^2}{4}\right) + \nu\gamma^2 \right] \tag{17}$$

$$\Gamma = \kappa_c g + \kappa g \tag{18}$$

where ω_0 is structural resonant frequency of the panel; ρ is structural density; Γ is panel aspect ratio; τ is thickness; E is Young’s modulus; ν is Poisson’s ratio; κ is dimensionless external excitation parameter; g is gravity, 9.81 m/s²; κ_c is the normalized magnitude of the acoustic pressure force in Equation (4) and given by:

$$\kappa_c = \frac{\rho_a \omega^2}{\rho g} \sum_u^U \sum_v^V \frac{\coth(\mu_{uv} c_i)}{\mu_{uv}} \frac{(\lambda_{uv})^2 \bar{A}}{\lambda_{\psi_{uv}} \lambda_{\varphi}} \tag{19}$$

Let \bar{s} be the solution of the following Duffing equation:

$$\frac{d^2 \bar{s}}{dt^2} + \left(\alpha + \frac{\Delta}{\Lambda} \right) \bar{s} + \beta \bar{s}^3 + \Gamma \cos(\omega t) = 0 \tag{20}$$

where $\bar{s} = \Lambda cn(\omega t)$; Λ is vibration magnitude; cn is elliptic cosine; Δ is a constant to be found. The elliptic cosine modulus is given by [20]:

$$k^2 = \frac{\beta \Lambda^2}{2 \left(\alpha + \frac{\Delta}{\Lambda} + \beta \Lambda^2 \right)} \tag{21}$$

The driving frequency in Equation (14) is equal to the response frequency of \bar{s} , which is given by:

$$\omega = \frac{2\pi}{\frac{4}{\left(\alpha + \frac{\Delta}{\Lambda} + \beta \Lambda^2\right)^{1/2}} \int_0^{\pi/2} \frac{1}{\sqrt{1-k^2 \sin^2(\theta)}} d\theta} \tag{22}$$

Consider Equation (14) and rewrite it into the following form:

$$\frac{d^2 s}{dt^2} + \left(\alpha + \frac{\Delta}{\Lambda} \right) s + \beta s^3 - \frac{\Delta}{\Lambda} s + \Gamma \cos(\omega t) = 0 \tag{23}$$

Then replace s by \bar{s} in Equation (23). The value on the right side is nonzero and considered as the residual:

$$\frac{d^2 \bar{s}}{dt^2} + \left(\alpha + \frac{\Delta}{\Lambda} \right) \bar{s} + \beta \bar{s}^3 - \Delta cn(\omega t) + \Gamma \cos(\omega t) = R(\Delta)$$

⇒

$$- \Delta cn(\omega t) + \Gamma \cos(\omega t) = R(\Delta) \tag{24}$$

The h th harmonic residual and overall residual are defined as:

$$R^h = \int_0^T R(\Delta) \cos(\omega t) dt \tag{25}$$

$$\bar{R} = \sqrt{\sum_{h=1,3,5\dots} (R^h)^2} \tag{26}$$

Note that the overall residual in Equation (24) also depends on Δ . Then, find the optimum value of Δ to minimize it, on the condition that the driving frequency in Equation (23) is equal to the response frequency of \bar{s} in Equation (22). Once the optimum value of Δ is found, the vibration magnitude Λ or \bar{A} can also be found. Hence, the magnitude of P_c in Equation (4) can be obtained. The transmission loss of a nonlinear flexible panel coupled with a partitioned cavity is defined by:

$$TL = -20 \log\left(\frac{|P_c|}{\kappa\rho g}\right) \tag{27}$$

where $|P_c|$ is the magnitude of the acoustic pressure.

Now, consider finding the peak frequency of damped case. According to the harmonic balance approximation approach in [19], the peak frequency can be found by the following equations:

$$\Lambda = \frac{\Gamma'}{\alpha' + \frac{3}{4}\beta\Lambda^2 + j(2\xi\omega\omega_p)} \tag{28}$$

Let $\Lambda = C + jD$:

$$C + jD = \frac{\Gamma'}{\alpha' + \frac{3}{4}\beta(C^2 - D^2) + j(2\xi\omega\omega_p + \frac{3}{2}\beta CD)} \tag{29}$$

where C and D are the real and imaginary parts of Λ ; ω_p is the peak resonant frequency; ξ is the damping factor; and j is complex number, $\sqrt{-1}$. Note that when considering a nonlinear flexible panel coupled with a partitioned cavity to find the peak frequency:

$$\alpha' = \omega_0^2 + \varepsilon \omega^2 \tag{30}$$

$$\Gamma' = \kappa g \tag{31}$$

$$\varepsilon = \frac{\rho_a \omega^2}{\rho} \sum_u^U \sum_v^V \frac{\coth(\mu_{uv} c_i)}{\mu_{uv}} \frac{(\lambda_{uv})^2}{\lambda_{\psi_{uv}} \lambda_{\varphi}} \tag{32}$$

Consider that the magnitude of Λ is maximum when $\omega = \omega_p$. Hence,

$$\alpha' + \frac{3}{4}\beta(C^2 - D^2) = 0 \tag{33}$$

Thus, Equation (29) is purely imaginary ($\therefore C = 0$)

$$\alpha' - \frac{3}{4}\beta D^2 = 0 \tag{34}$$

$$iD = \frac{\Gamma'}{i(2\xi\omega\omega_p)} \tag{35}$$

Hence, the peak frequency ω_p , can be obtained by solving Equations (34) and (35).

3. Results and Discussion

Figure 2 shows the comparison between the frequency response curves obtained from the proposed method and the modified residue harmonic balance method [18]. The results obtained from the two methods reasonably agree with each other. The main discrepancy occurs (1) at very low frequency ($\omega \approx 0.6\sqrt{\alpha}$), where the two solution curves intercept; and (2) at very high frequency ($\omega > 5\sqrt{\alpha}$), the nonlinear solution curve from the proposed method is slightly lower. It is noted that the super harmonic solution of the proposed method is obtained by setting the response frequency equal to $3 \times$ driving frequency. In the following case studies, the configurations and material properties of the nonlinear panel are: 200 mm \times 200 mm \times 1 mm aluminum panel, Young's modulus $E = 7 \times 10^{10}$ N/m²,

Poisson's ratio $\nu = 0.3$, and panel mass density $\rho = 2700 \text{ kg/m}^3$. Tables 1 and 2 show the mode convergences and harmonic contributions for various driving frequencies. It can be seen that the nine-mode approximation can achieve three digital accuracies. When the driving frequency is higher, the higher harmonic components of the elliptic cosine solution form are more significant. In Table 2, it is found that when the driving frequency is near or above the first resonant frequency, the fundamental harmonic component is always dominant (over 90%); when the driving frequency is far below the first resonant frequency and the excitation level is higher (e.g., $k = 150$) and the higher harmonic components would be more significant. When a harmonic balance method is adopted for such case, there would be more nonlinear coupled equations generated in the harmonic balance procedures. It is due to more harmonic terms being required. As aforementioned, the main advantage of the proposed approach is that one elliptic cosine contains various harmonic components, while one simple cosine term carries one particular harmonic component. That is why the proposed solution form can be more concise than those in the harmonic balance procedures. Figures 3 and 4 show the panel amplitude and transmission loss plotted against the excitation frequency for various excitation magnitudes, respectively. In Figures 3 and 4, the peak frequency increases with the excitation magnitude. The bigger the excitation magnitude is, the longer the nonlinear solution curve extends. In the case of small excitation magnitude, the amplitude peak and transmission loss dip are much more symmetric. In Figure 3, the differences between the amplitude curves of the four different excitation magnitudes are obvious. On contrary, in Figure 4, the differences between the transmission loss curves of the four different excitation magnitudes are almost undetectable in the linear and low frequency nonlinear cases. The tips of the nonlinear solution curves are far from each other. Note that according to the linear theory, the resonant peak frequencies and transmission loss dips are independent of excitation magnitude. In Figure 3, the nonlinear solution curve of $k = 50$ appears as a straight line with a shallow slope (note the excitation magnitude in this case is very large). The super harmonic solution curve is the longest one. There is an interesting finding in Figure 4. The overall slopes of the nonlinear and super harmonic transmission curves of $k = 50$ are also quite shallow. Unlike those of other curves, the upper and lower limits of them are only about $\pm 8 \text{ dB}$. It is implied that under very large excitation, the nonlinear panel sound transmission would not vary largely for different driving frequencies. Besides, it is found that in the case of the smallest excitation magnitude, there is a narrower transmission loss dip and a higher dip value; and in the case of the biggest excitation magnitude, the nonlinear vibration would widen the transmission loss dip and decrease the dip value. From this observation, for wideband excitation, the nonlinear vibration would make the overall transmission loss worse; and for narrowband excitation (near the resonant frequency), the linear vibration would make the overall transmission loss worse. The negative effect of the super harmonic response would be minimal when the excitation magnitude is small. Figures 5 and 6 show the panel amplitude and transmission loss plotted against the excitation frequency for various cavity depths, respectively. It is found that a longer cavity depth would induce a lower transmission loss peak frequency, and a higher transmission loss dip value. In the linear amplitude solution cases, the three curves are drawing closer when the driving frequency is higher. Unlike those in Figure 5, the linear transmission loss curves in Figure 6 are nearly parallel to each other for their frequency range. In the case of the shortest cavity depth, the tip values of the super harmonic amplitude and transmission loss curves are significantly smaller. It is due to the damping effect, which depends on the corresponding dip frequency, that it is much stronger. Besides, the nonlinear amplitude curve and linear transmission loss solution curve are the lowest. It is implied that the amplitude is the smallest due to the highest stiffness for that low frequency range, and the sound reduction capacity of the panel is the weakest for the high frequency range. Note that the nonlinear transmission loss solution curve is the lowest only for the dimensionless driving frequency less than one and higher than two. The linear amplitude solution curve is the highest one. This is implied that the overall stiffness is the weakest in the linear solution case.

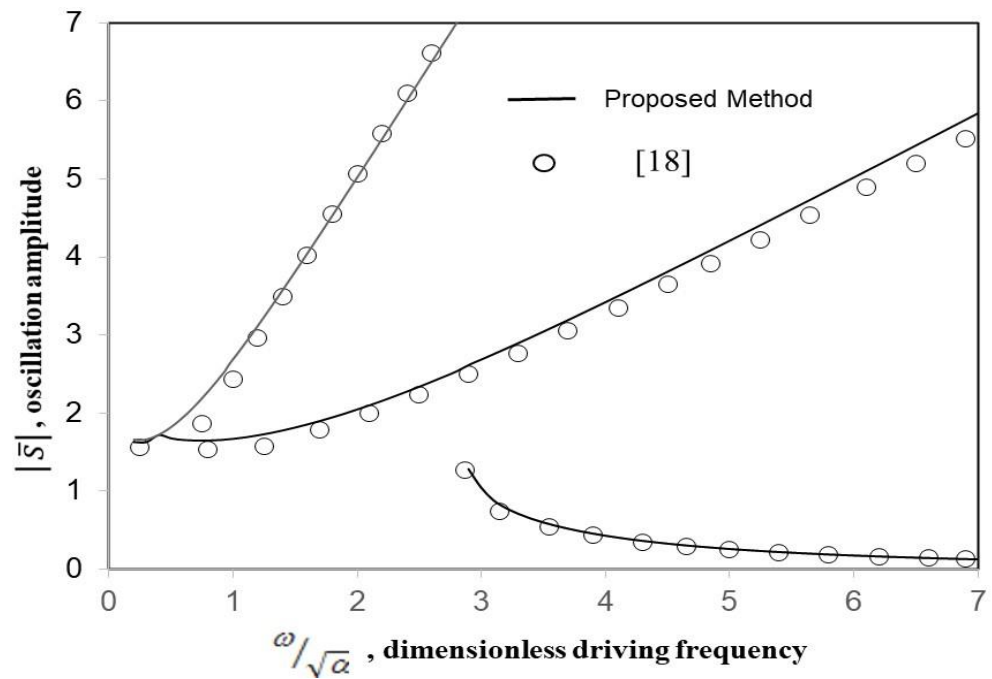


Figure 2. Comparison between the frequency response curves obtained from the proposed method and [18] ($\alpha = 1, \beta = 2, \Gamma = 6$).

Table 1. Vibration amplitude convergence for various driving frequencies and number of modes used ($c/a = 0.5, k = 10, \zeta = 0$).

	$\omega/\omega_0 = 1$	$=2$	$=3$
1 acoustic mode	0.2666	1.6386	2.8236
4 acoustic modes	0.2681	1.6442	2.8312
9 acoustic modes	0.2681	1.6443	2.8313
16 acoustic modes	0.2681	1.6443	2.8314

Table 2. Harmonic contributions of the elliptic cosine solution form for various driving frequencies ($c/a = 0.5, \zeta = 0$).

$k = 10$	$\omega/\omega_0 = 1/3$	$=1$	$=2$
1st harmonic ($h = 1$)	99.5090	99.7035	97.1538
2nd harmonic ($h = 3$)	0.4887	0.2957	2.7674
3rd harmonic ($h = 5$)	0.0024	0.0009	0.0767
4th harmonic ($h = 7$)	0.0000	0.0000	0.0021
$k = 150$	$\omega/\omega_0 = 1/3$	$=1$	$=2$
1st harmonic ($h = 1$)	61.9037	93.1036	95.7717
2nd harmonic ($h = 3$)	26.2178	6.4492	4.0565
3rd harmonic ($h = 5$)	8.9249	0.4198	0.1651
4th harmonic ($h = 7$)	2.9536	0.0274	0.0067

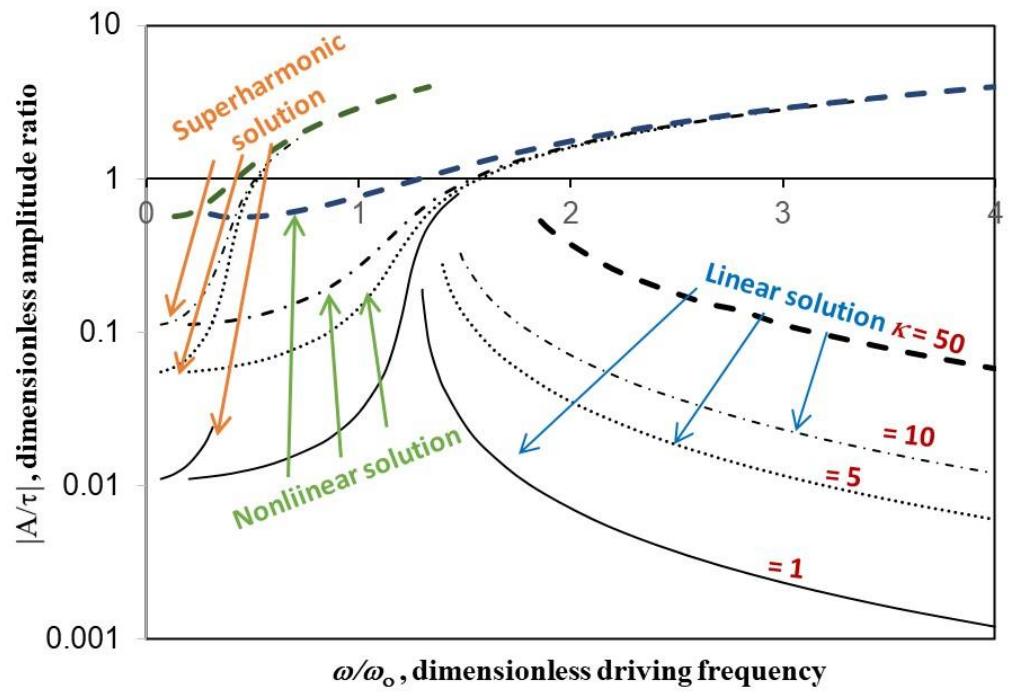


Figure 3. Amplitude ratio versus excitation frequency for various excitation magnitudes ($c/a = 0.5$, $\zeta = 0.02$, single cavity).

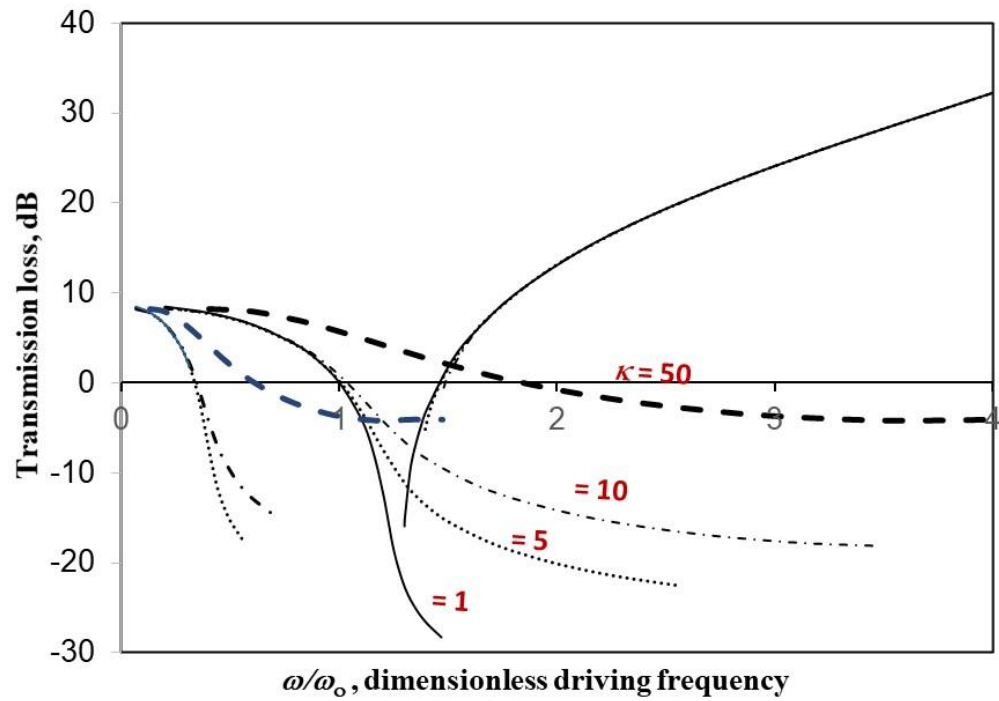


Figure 4. Transmission loss ratio versus excitation frequency for various excitation magnitudes ($c/a = 0.5$, $\zeta = 0.02$, single cavity).

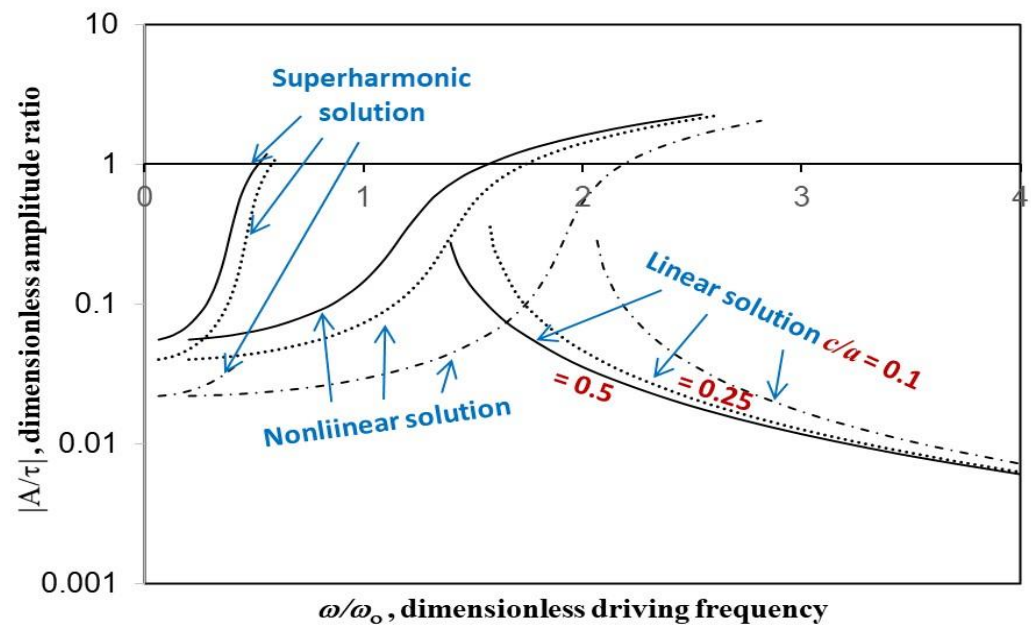


Figure 5. Amplitude ratio versus excitation frequency for various cavity depths ($k = 5, \zeta = 0.02$, single cavity).

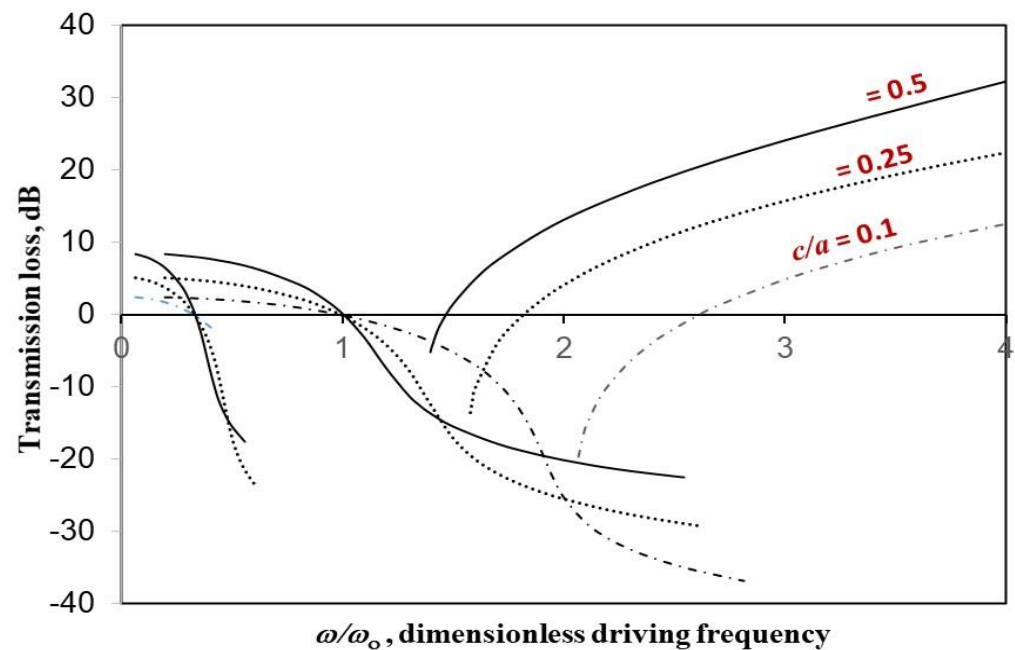


Figure 6. Transmission loss ratio versus excitation frequency for various cavity depths ($k = 5, \zeta = 0.02$, single cavity).

Figures 7 and 8 show the panel amplitude and transmission loss plotted against the excitation frequency for various partitioned cavity cases, respectively. The average cavity depths in the three cases are the same. The patterns of the solution curves in Figures 7 and 8 are very similar to those in Figures 5 and 6. The solution curves of the partitioned cavity with unequal cavity depths and the partitioned cavity with equal cavity depths are analogous to those of the shortest and second shortest cavity depths in Figures 5 and 6, respectively. The depths of the partitioned cavity with unequal cavity depths are 50 mm, 200 mm, and 50 mm respectively. There are two partitioned cavities with depth of 50 mm, where the stiffnesses are much stronger and thus, the overall stiffness is also the strongest. Besides, the overall stiffness of three smaller cavities is higher than that of one big cav-

ity. That is why the solution curves of the partitioned cavity with equal cavity depths in between those of other two cases.

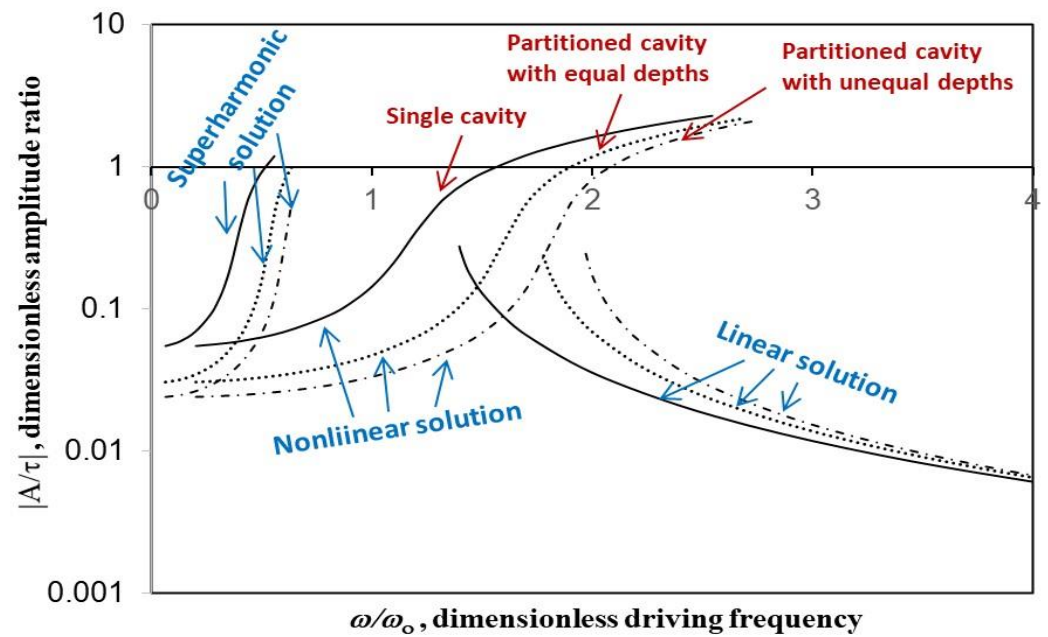


Figure 7. Amplitude ratio versus excitation frequency for various cavity cases ($c/a = 0.5$, $k = 5$, $\zeta = 0.02$).

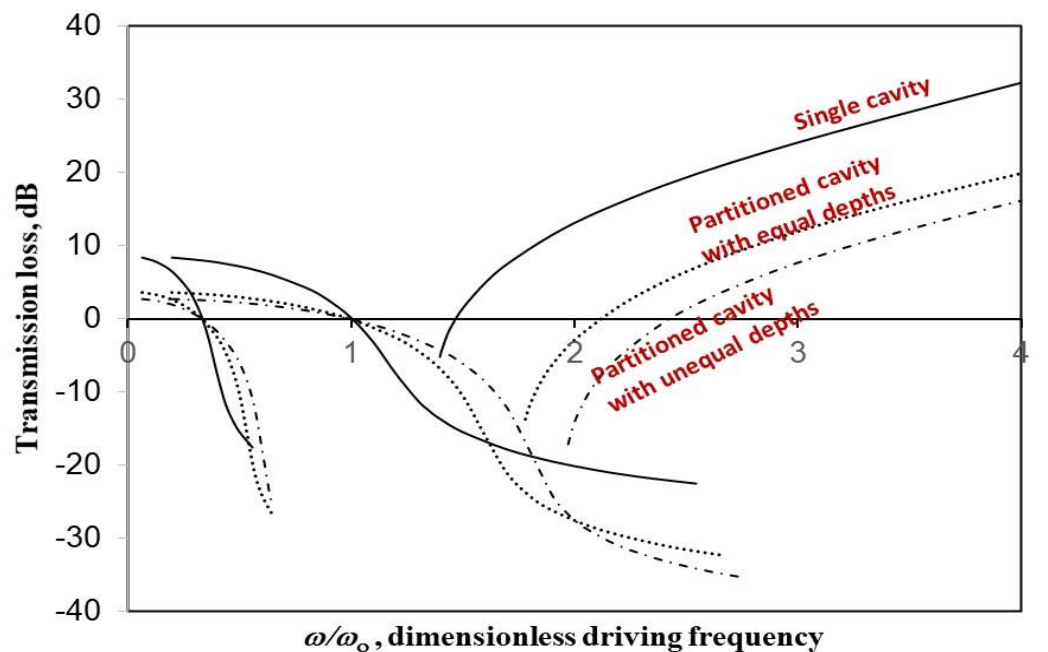


Figure 8. Transmission loss versus excitation frequency for various cavity cases ($c/a = 0.5$, $k = 5$, $\zeta = 0.02$).

Figures 9–11 show the waveform differences for various cases, respectively. It can be seen that in the nonlinear solution case of $k = 50$, the maximum difference between the elliptic cosine and simple cosine is about 40%. It is much bigger than that in the linear case (smaller than 0.1%). As aforementioned, one elliptic cosine contains various harmonic components, while one simple cosine just carries one particular harmonic component. That is why the solution form in the proposed method can be more concise than those in other harmonic balance methods which need more sine or cosine terms. Figure 12 shows

the elliptic cosine waveforms of different excitation magnitudes. It can be seen that the waveform of $k = 50$ looks like a triangle; and the troughs in the waveforms of $k = 100$ and 150 are very narrow. All these waveforms are very different from the simple cosine (i.e., $k = 0$) and contain significant higher harmonic components.

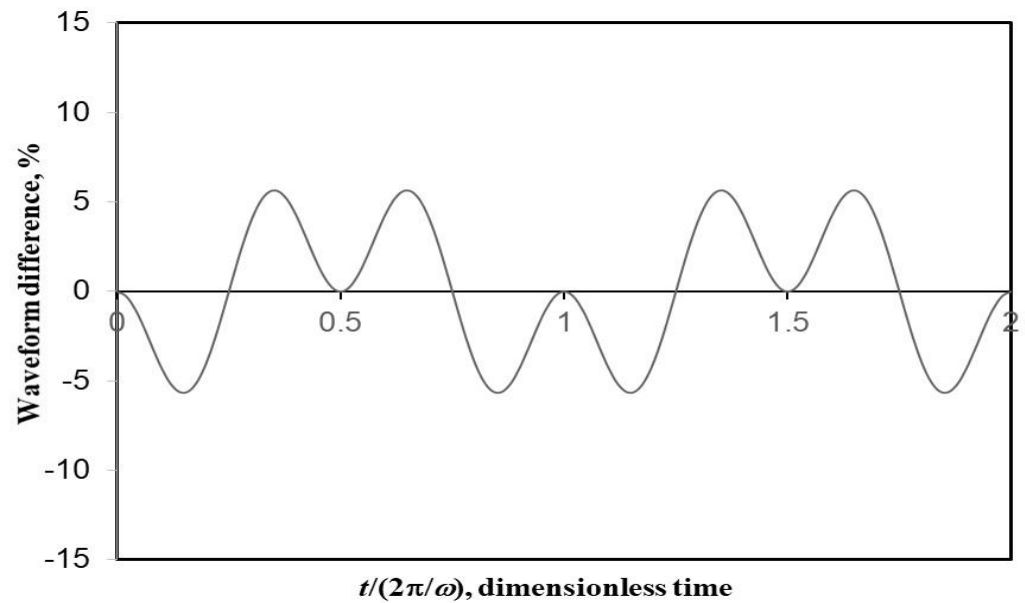


Figure 9. Difference between elliptic cosine and simple cosine ($c/a = 0.5$, $k = 5$, $w/w_0 = 3$, $\zeta = 0.02$, single cavity, nonlinear solution).

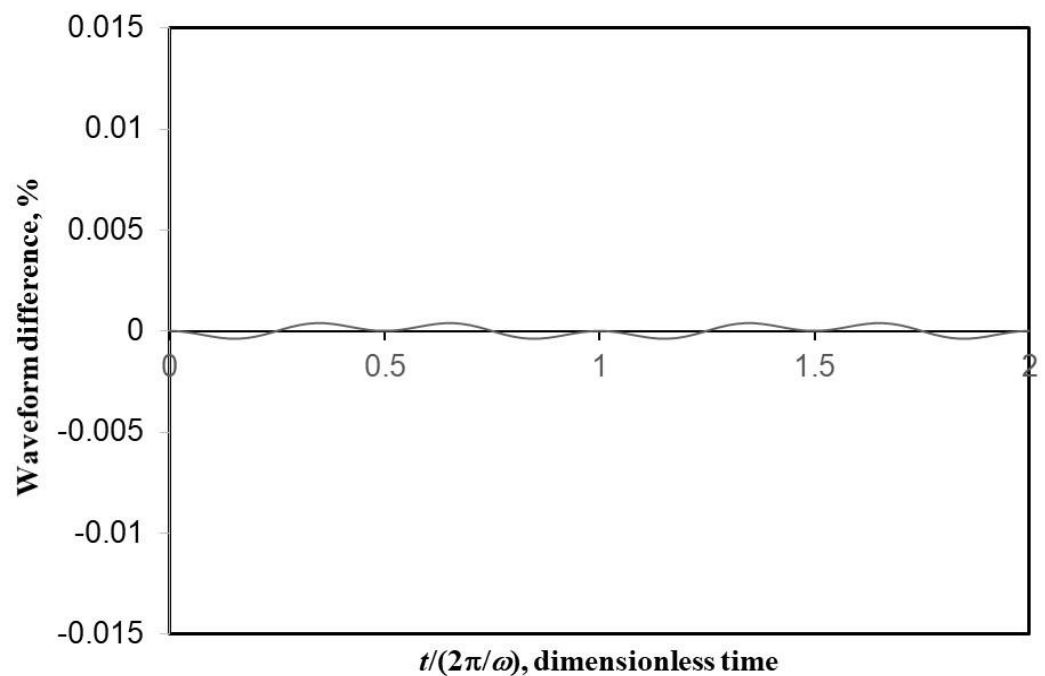


Figure 10. Difference between elliptic cosine and simple cosine ($c/a = 0.5$, $k = 5$, $w/w_0 = 3$, $\zeta = 0.02$, single cavity, linear solution).

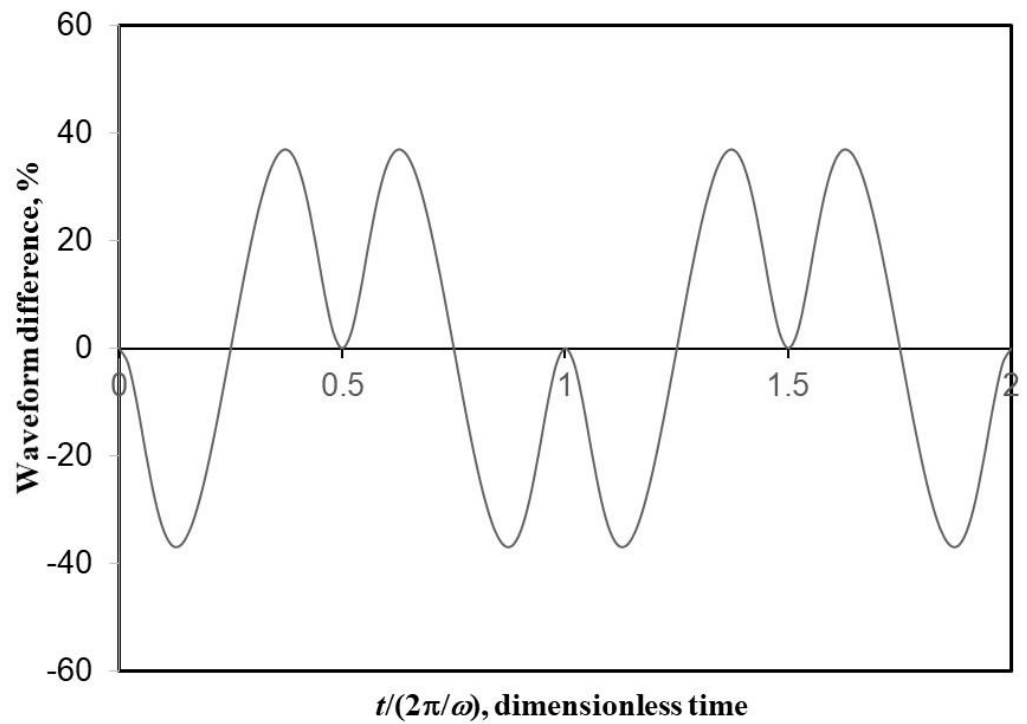


Figure 11. Difference between elliptic cosine and simple cosine ($c/a = 0.5, k = 50, w/w_0 = 3, \zeta = 0.02$, single cavity, nonlinear solution).

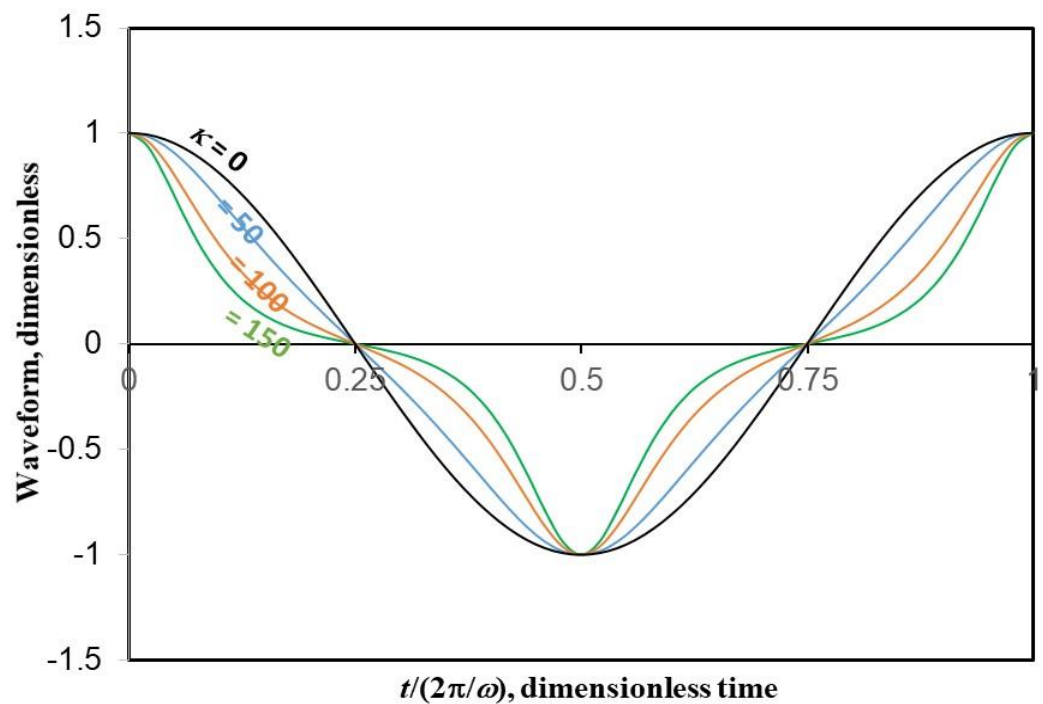


Figure 12. Elliptic cosine waveform ($c/a = 0.5, w/w_0 = 3, \zeta = 0.02$, single cavity, nonlinear solution).

4. Conclusions

This study has analyzed the forced vibration and transmission loss of a nonlinearly vibrating panel backed by a partitioned cavity. The proposed elliptic integral method is newly applied to this nonlinear vibro-acoustic problem. The nonlinear structural/acoustic modal formulation has been developed from the well-known wave equation and Duffing equation. The results obtained from the proposed method and modified residue harmonic

balance method are reasonably consistent. The effects of some parameters on the vibration responses and transmission loss performances are investigated. The main findings include (1) for wideband excitation, the nonlinear vibration would make the overall transmission loss worse, (2) for narrowband excitation (near the resonant frequency), the linear vibration would make the overall transmission loss worse; and (3) the stiffness of a system with a partitioned cavity with unequal cavity depths is the strongest among the three cases considered. It is the easiest for a sound pressure to transmit through the panel, so that the transmission loss performance is generally the worst.

Funding: This research received no external funding.

Informed Consent Statement: Not applicable.

Data Availability Statement: No additional data available.

Conflicts of Interest: The author declares no conflict of interest.

References

1. Isaac, C.W.; Pawelczyk, M.; Wrona, S. Comparative Study of Sound Transmission Losses of Sandwich Composite Double Panel Walls. *Appl. Sci.* **2000**, *10*, 1543. [\[CrossRef\]](#)
2. Lin, H.J.; Wang, C.N.; Kuo, Y.M. Sound transmission loss across specially orthotropic laminates. *Appl. Acoust.* **2007**, *68*, 1177–1191. [\[CrossRef\]](#)
3. Thamburaj, P.; Sun, J.Q. Optimization of anisotropic sandwich beams for higher sound transmission loss. *J. Sound Vib.* **2002**, *254*, 23–36. [\[CrossRef\]](#)
4. Chen, Y.Z.; Lin, X.Y. A convenient technique for evaluating angular frequency in some nonlinear oscillations. *J. Sound Vib.* **2007**, *305*, 552–562. [\[CrossRef\]](#)
5. Sun, M.; Quan, T.T.; Wang, D.M. Nonlinear oscillations of rectangular plate with 1:3 internal resonance between different modes. *Results Phys.* **2018**, *11*, 495–500. [\[CrossRef\]](#)
6. Rahman, M.S.; Haque, M.E.; Shanta, S.S. Harmonic balance solution of nonlinear differential equation (Non-conservative). *Adv. Vib. Eng.* **2010**, *9*, 345–356. [\[CrossRef\]](#)
7. Mickens, R.E. A generalization of the method of harmonic balance. *J. Sound Vib.* **1986**, *111*, 515–518. [\[CrossRef\]](#)
8. Moreno-Pulido, S.; Garcia-Pacheco, F.J.; Sanchez-Alzola, A.; Rincon-Casado, A. Convergence Analysis of the Straightforward Expansion Perturbation Method for Weakly Nonlinear Vibrations. *Mathematics* **2021**, *9*, 1036. [\[CrossRef\]](#)
9. Wu, Y.; He, J.H. Homotopy perturbation method for nonlinear oscillators with coordinate-dependent mass. *Results Phys.* **2018**, *10*, 270–271. [\[CrossRef\]](#)
10. Rafei, M.; Van Horssen, W.T. Solving systems of nonlinear difference equations by the multiple scales perturbation method. *Nonlinear Dyn.* **2012**, *69*, 1509–1516. [\[CrossRef\]](#)
11. Lyon, R.H. Noise reduction of rectangular enclosures with one flexible wall. *J. Acoust. Soc. Am.* **1963**, *35*, 1791–1797. [\[CrossRef\]](#)
12. Pretlove, A.J. Free vibrations of a rectangular panel backed by a closed rectangular cavity. *J. Sound Vib.* **1965**, *2*, 197–209. [\[CrossRef\]](#)
13. Jackson, R.S. Some aspects of the performance of acoustic hoods. *J. Sound Vib.* **1966**, *3*, 82–94. [\[CrossRef\]](#)
14. Ortiz, S.; Gonzalez, C.; Cobo, P.; de Espinosa, F.M. Attenuating open cavity tones by lining its walls with microperforated Panels. *Noise Control Eng. J.* **2014**, *62*, 145–151. [\[CrossRef\]](#)
15. Sadri, M.; Younesian, D. Vibroacoustic analysis of a sandwich panel coupled with an enclosure cavity. *Compos. Struct.* **2016**, *146*, 159–175. [\[CrossRef\]](#)
16. Hu, Z.Y.; Maxit, L.; Cheng, L. Convergence criteria on the acoustic velocity continuity in a panel-cavity system. *J. Acoust. Soc. Am.* **2017**, *141*, 2137–2142. [\[CrossRef\]](#)
17. Sum, K.S.; Pan, J. Study of the medium frequency response of sound field in a panel-cavity system. *J. Acoust. Soc. Am.* **1998**, *103*, 1510–1519. [\[CrossRef\]](#)
18. Lee, Y.Y. Multi-Level residue harmonic balance method for the transmission loss of a nonlinearly vibrating perforated panel. *Int. J. Struct. Stab. Dyn.* **2016**, *16*, 1450100. [\[CrossRef\]](#)
19. Lee, Y.Y. The effect of large amplitude vibration on the pressure-dependent absorption of a structure multiple cavity system. *PLoS ONE* **2019**, *14*, e0219257. [\[CrossRef\]](#)
20. Lee, Y.Y. Free vibration analysis of nonlinear structural-acoustic system with non-rigid boundaries using the elliptic integral approach. *Mathematics* **2020**, *8*, 2150. [\[CrossRef\]](#)
21. Hsu, C.S. On the application of elliptic functions in nonlinear forced oscillations. *Q. Appl. Math.* **1960**, *17*, 393–407. [\[CrossRef\]](#)
22. Alvaro, H.S.; Jairo, E.C.H. Exact solution to Duffing equation and the pendulum equation. *Appl. Math. Sci.* **2014**, *8*, 8781–8789.
23. Vahidi, A.R.; Babolian, E.; Cordshooli, G.A. Numerical solutions of Duffing's oscillator problem. *Indian J. Phys.* **2012**, *86*, 311–315. [\[CrossRef\]](#)
24. El-Naggar, A.M.; Ismail, G.M. Analytical solution of strongly nonlinear Duffing oscillators. *Alex. Eng. J.* **2016**, *55*, 1581–1585. [\[CrossRef\]](#)

25. Qaisi, M.I. Analytical solution of the forced Duffing's oscillator. *J. Sound Vib.* **1996**, *194*, 513–520. [[CrossRef](#)]